Azimuthons and pattern formation in annularly confined exciton-polariton Bose-Einstein condensates

Guangyao Li
Nonlinear Physics Centre, Research School of Physics and Engineering, Australian National University, Canberra, Australian Capital Territory 0200, Australia

(Received 6 November 2015; published 20 January 2016)

We present numerical analysis of steady states in a two-component (spinor) driven-dissipative quantum fluid formed by condensed exciton polaritons in an annular optically induced trap. We demonstrate that an incoherent ring-shaped optical pump creating the exciton-polariton confinement supports the existence of stationary and rotating azimuthon steady states with azimuthally modulated density associated with Josephson vortices. Such states can be imprinted by coherent light pulses with a defined orbital angular momentum, as well as generated spontaneously in the presence of thermal noise.

DOI: 10.1103/PhysRevA.93.013837

I. INTRODUCTION

The dynamics of open-dissipative exciton-polariton condensates in optically defined trapping potentials has developed into an active area of research due to a high degree of flexibility and scalability afforded by the optical trapping techniques [1,2]. Annular confinement in particular is capable of supporting superfluid polariton currents, which are of potential use for proposed interferometry and sensing devices based on microcavity polaritons [3]. The annular polariton flow, its stability and disruption [4–6], and its connection to nontrivial vortices in two-component (spinor) polariton systems [7] have been vigorously investigated both experimentally and theoretically. The spin degree of freedom of a microcavity polariton is directly linked to the polarization of its photonic component and therefore can be easily mapped out via polarization and frequency-resolved optical tomography of cavity photoluminescence. This straightforward detection method has enabled a multitude of experimental studies of half solitons, half vortices, spin vortices, and other nontrivial spin textures spontaneously occurring in exciton-polariton condensates [7–12].

The majority of nontrivial spin dynamics in polariton condensates is associated with the Rashba-like coupling between the spin components introduced by the effective magnetic field induced by the momentum-dependent TE-TM energy splitting between the polariton modes [13,14]. However, spontaneous formation of spin patterns and nontrivial spin dynamics [15,16] can also be caused by the asymmetry-induced momentum-independent linear coupling between the circular polarization components, which commonly arises due to the strains in the semiconductor heterostructures.

In this work we examine nontrivial spin states of the dynamical system describing a nonequilibrium, incoherently pumped Bose-Einstein condensate (BEC) of exciton polaritons trapped by an annular potential induced by the pump. We show that this pumping configuration supports steady vortex states with azimuthally modulated density (azimuthons), which can be interpreted as Josephson vortices [17–20]. Steady rotation with terahertz (THz) -range frequency associated with these states results in an optical ferris wheels [21] in cavity photoluminescence. Recently, it was shown that two polariton condensation centers can exhibit self-induced oscillations that cover a wide range of frequency [22]. Thus, the optical ferris wheels can be viewed as spin oscillations at the THz range being manifested in the spatial domain. We also describe the stationary pattern formation supported by nonlinear instabilities of the annular polariton flow and show that the noise naturally present in the system due to, for example, thermal effects allows for spontaneous formation of vortex azimuthons.

II. MODEL

The mean-field dynamics of a two-component (spinor) polariton condensate can be described by the open-dissipative Gross-Pitaevskii (GP) equation coupled to the rate equations for a spin-polarized reservoir of hot excitonic polaritons created and replenished by a nonresonant optical pump [9,23]. In the circularly polarized basis $\psi_\pm$, where $+$ and $-$ stand for the right- and left-hand circular polarization components, respectively, the dynamical model is written as follows ($\sigma = \pm$):

$$\begin{aligned} i\partial_t\psi_\sigma &= \left\{-\frac{1}{2}\nabla^2 + u_a|\psi_\sigma|^2 + u_b|\psi_{-\sigma}|^2 + g_R n_\sigma \right. \\ &\quad \left. + \frac{i}{2}[R n_\sigma - \gamma_c]\right\}\psi_\sigma + J\psi_{-\sigma}, \\ \partial_t n_\sigma &= P_\sigma(r) - (\gamma_R + R|\psi_\sigma|^2)n_\sigma, \end{aligned} \tag{1}$$

where u_a and u_b represent ($|u_b| < |u_a|$ [24]) the same-spin and cross-spin s-wave scattering strengths, respectively, g_R characterizes interactions between the condensate and reservoir (the blueshift energy), R is the same-spin stimulated scattering rate from the reservoir into the condensate, γ_c is the loss rate of polaritons with $\gamma_c = 1/\tau_c$ where τ_c is the polariton lifetime, and J is the internal Josephson coupling. For the reservoir equation, n_σ is the spin-dependent reservoir density [9], P_σ is the spin-dependent pumping rate, and γ_R is the loss rate of the reservoir polaritons. The anisotropic TE-TM splitting effect is assumed to be weak and thus is not taken into account [25]. We also assume that the cross-spin stimulated scattering is negligible compared with the same-spin counterpart [15]. As shown in [16], weak cross-spin stimulated scattering will not significantly affect the spin dynamics. In experiments, the polariton condensate can either separate from the reservoir

 ©2016 American Physical Society

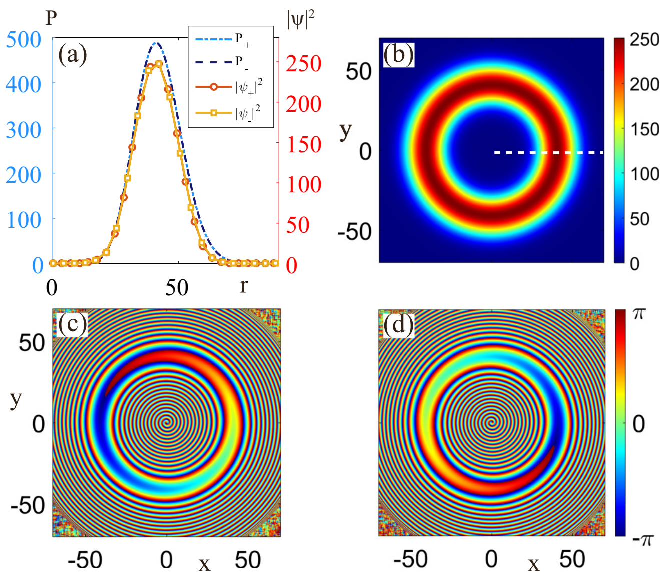

FIG. 1. Antibonding states formed under a LG_{50} mode pumping. (a) Radial profiles of the condensate density and pumping rate along the dashed line in (b). (b) Density distribution of the + component. (c) Phase distribution of the − component. (d) Phase distribution of the + component. The parameters are $\bar{P} = 6$, $P_L = 0.5$, and $J = 0.5$.

in space or not. For the former case, a detailed study of its spin dynamics can be found in [26]; here we will only discuss the latter case where the condensate spreads over the whole pumping area.

Equation (1) is written in the dimensionless form by using the characteristic scales of time $\tau_c = 3$ ps, length $L = \sqrt{\hbar/m\gamma_c} = 2$ μm, and energy $E_u = \hbar\gamma_c = 0.66$ meV. We assume a parabolic dispersion approximation near the polariton ground state, where m is the effective mass of the lower polaritons. All unspecified parameters in Eq. (1) take the default numerical values in [27]. For these parameters, the unit of time $t = 1$, used in dynamical simulations throughout this work, corresponds to 3 ps. All quantities in Figs. 1–7 are plotted in dimensionless units.

Although generally the energy functional corresponding to Eq. (1) takes complex values, when the pumping and decay reach equilibrium there exist dynamically stable steady states whose energy functionals are strictly real [6]. This suggests that the condensate dynamics can be approximately characterized by the real part of the energy functional [28], which remains unchanged when a steady state or a vortex azimuthon is reached, where for the former the pumping and dissipation compensate each other at every moment, whereas for the latter the same equilibrium is reached only on average.

Under the incoherent pumping conditions, the phase of the pump beam will be lost during the polariton energy relaxation process due to scattering with phonons. The spatial distribution of the condensate therefore is controlled by the pump rate $P_\sigma(r)$, which is proportional to the spatial intensity distribution of the pump beam. In this work we use a Laguerre-Gaussian (LG) beam to form an annular pumping configuration. The pumping power of the beam is normalized by the threshold power for polariton condensation $\bar{P} = P^{\max}/P_{\text{th}}$, where $P_{\text{th}} = \gamma_R\gamma_c/R$ is the pumping threshold given by the homogeneous pump approximation [23] and $P^{\max}$ is the peak intensity of the LG beam. For a spinor system, the intensity of the LG beam is split into each component as $\bar{P} = \bar{P}_+ + \bar{P}_-$. We denote the polarization bias of the pump by $P_L = \bar{P}_-/\bar{P}$, which represents the fraction of power in the − component, e.g., for a linearly polarized pump $P_L = 0.5$, while for a right-handed circularly polarized pump $P_L = 0$.

In the following sections, all simulation results are given by solving Eq. (1) via the split-step method [29].

III. VORTEX STATES

The full picture of dynamical phenomena described by Eq. (1) is given by the interplay between the nonlinear interactions and the linear coupling. We start the discussion by reviewing some of the existing results as limiting cases of the dynamical model and then extend our understanding to the more intricate situations.

If $J = 0$ and the cross-spin nonlinear interaction is vanishingly small, two polarization components become effectively decoupled from each other and Eq. (1) reduces to two sets of single-component equations. To obtain a steady state, one can require the equilibrium between pumping and decay $Rn_\sigma - \gamma_c = 0$ and steady reservoir density $\partial_t n_\sigma = 0$. Together these conditions lead to $|\psi_\sigma|^2 \propto P_\sigma$, i.e., the condensate density distribution follows the intensity distribution of the pump and is therefore azimuthally homogeneous. Under a LG pump P_σ, the condensate density distribution has an annular shape that can support vortex states. A detailed discussion of the existence and stability properties of single-component vortex states can be found in Ref. [6]. These states are modulationally stable in certain parameter regimes and in what follows we will consider only these regimes.

The above conclusion remains valid even in the presence of the cross-spin interaction [15]. Thus, the topological charges of vortex states for each polarization component can be different from each other. When the condensate is pumped by a linearly polarized ($P_L = 0.5$) LG beam and one component acquires nonzero angular momentum, e.g., $m_+ = 1$ and $m_- = 0$, where m is the topological charge [6], the system forms the so-called half-vortex state [30,31], which has been observed in experiment [8]. When viewed in the linearly polarized basis, such a state forms a rotating vortex with a π phase jump around the azimuthal coordinate and a density dip [32], where the horizontal and vertical polarization components in the linearly polarized basis are defined, respectively, as

$$\psi_H = \frac{1}{\sqrt{2}}(\psi_+ + \psi_-), \quad \psi_V = \frac{i}{\sqrt{2}}(\psi_- - \psi_+). \tag{2}$$

If $J \neq 0$ (without lost of generality we assume $J > 0$ throughout this work), there exists an energy splitting between two polarization components [33], which will lead to particle exchange between ψ_+ and ψ_-, the so-called Josephson currents [see Eq. (5)], and will introduce spin dynamics into our system [34]. Assuming that the spatial variation of the condensate can be ignored (the homogeneous approximation), previous studies have shown that, under a linearly polarized ($P_L = 0.5$) pump, with sufficiently large J, the condensate will fall into the antibonding state, where the relative phase between the two components maintains a π difference [16]. Now we model the pumping configuration with a linearly polarized LG beam whose cross-section profile is shown in Fig. 1(a). The condensate falls into the antibonding state with a spatially inhomogeneous density distribution. The relative phase between the two components maintains a π difference over the whole pumping region, and if one component forms a vortex state with the topological charge $m = 1$, the fixed phase difference will drag the other component into the same vortex state with an overall π phase lapse (see Fig. 1). This is a static half-vortex state: when viewed in the linearly polarized basis, the state does not rotate.

The above two cases are two-component stable vortex states given by a simple combination of previous results and they form the qualitative description of our system. When J is weak, two components are loosely coupled; when J is large, they maintain a fixed relative phase, regardless of their spatial distribution. The angular momentum acquired by each component can be imprinted by a coherent LG pulse in the initial state [35]. The coherent phase imprinting enforces the formation of predetermined vortex states. However, as demonstrated in Sec. VI, with a suitable pumping configuration, vortex states can also form spontaneously from white noise.

IV. AZIMUTHONS

Vortex states in the annular trap created by the optical LG pump have azimuthally homogeneous density distributions and azimuthally linear phase distributions over the pumped area. It has been shown previously, for both the conservative GP model and the nonlinear Schrödinger and Ginsburg-Landau models in optics, that vortex states are special cases of more general steady states with periodic azimuthal density modulations that have been realized in optics as azimuthons and in atomic BEC system as soliton train (ST) states. Various types of azimuthons have been studied extensively [36–38] and have been observed in experiments [39,40]. The notion of vortex azimuthons has recently been extended to open-dissipative systems [41–44]. For conservative (atomic) BEC systems, the analytical expression for the ST state was first developed in [45,46]. Since then the ST states have been considered both for the single-component case [47] and for the two-component case [48,49]. Note that in literature the term "soliton train" might refer to a series of propagating solitons under the open-boundary condition [50]. Here the ST state refers to the one [47,48] with the periodic boundary condition. In the following, within the scope of our discussion, we will not discriminate between the azimuthon and the ST state. (Detailed comparisons can be found in [36,47].)

Stable ST states in a single-component polariton system under the incoherent LG pumping scheme are not possible as a result of the driven-dissipative nature of the system. As mentioned above, a steady-state condensate and reservoir density distribution should be proportional to the pump rate, i.e., for an annular azimuthally homogeneous pump their density should be azimuthally homogeneous. This argument no longer holds true if the system supports Josephson vortices [17–20] that stem from internal Josephson currents between the two condensate components. In the simplest case, a Josephson vortex will introduce a sine-shape spatial distribution of Josephson current between two components [18]. If the Josephson vortex does not fully compensate the density difference between the two components, one can expect that the density modulation of a vortex state will form cnoidal waves [51] that mimic the conservative soliton state.

The particle density imbalance can be introduced by a spin-biased pump. The homogeneous spin dynamics considered in [16] dictates that, if the polarization of the pump slightly deviates from the linear one ($P_L = 0.5$), the condensate will still form a steady state with a fixed relative phase that is close to but not exactly π. We refer to such a state as a semiantibonding (SAB) state and the corresponding relative phase is denoted by θ_s. The relative phase between ψ_+ and ψ_- is defined by

$$\theta(\mathbf{r},t) = \phi_-(\mathbf{r},t) - \phi_+(\mathbf{r},t), \tag{3}$$

where $\phi_\pm$ is the phase of $\psi_\pm$. In such a state, the Josephson current maintains the relative phase θ_s between two components throughout the whole pumped area. In an annular pumping configuration, if both components acquire nonzero angular momentum $m_\pm$ (not necessarily the same), the spatial flow of the condensate will lead to spatial variation of the phase in each polarization component. This variation is governed by the relation $\mathbf{v} \sim \nabla\phi$, where $\mathbf{v}$ is the velocity of the condensate flow and ϕ is the phase, and will lead to the deviation of the relative phase between the components from θ_s. The competition between the azimuthal flow governed by the nonlinear interactions within each component and the Josephson current given by the linear coupling between the two components results in cnoidal rotating waves that are very similar to that of the ST states found in atomic BEC systems.

Figure 2 shows a snapshot of the ST state. In this case, the + component was pumped more strongly than the − component, which is demonstrated by the pseudocolor representation of the polariton density. Although each component acquired different angular momentum $m_+ = -2$ and $m_- = 1$, their densities rotated in the same direction as indicated by the white arrows. Density dips can be seen in their density distribution for both components. The number of density dips is given by the phase winding difference between the two components, and in the current case specifically $j = |m_+ - m_-| = 3$. The ST state is spatially inhomogeneous and the dimensionality reduction method used in [6] is no longer applicable. Nevertheless, the condensate can be qualitatively represented by the area pumped most strongly by the LG beam, as indicated by the white dashed ring in Fig. 2(a). Figure 2(f) shows the density and phase distribution around the dashed ring for both components. The Josephson current cannot fully compensate the density difference around the ring and the azimuthal density dip distributions in the two components are complementary and are associated with the azimuthally nonlinear distribution of phase. Figure 2(c) further demonstrates that the ST state is stable to a weak broadband perturbation defined in [6].

To verify cnodial wave rotations, Fig. 3(a) shows time series of the condensate density recorded along the dashed ring, which demonstrates the periodic rotation around the center of the condensate, with the period at about $T_P \sim 10$ ps, at the frequency of terahertz. Figure 3(b) shows the instantaneous density and phase distribution for ψ_+ along the dashed ring, as well as plots fitted by using the expression for cnoidal waves

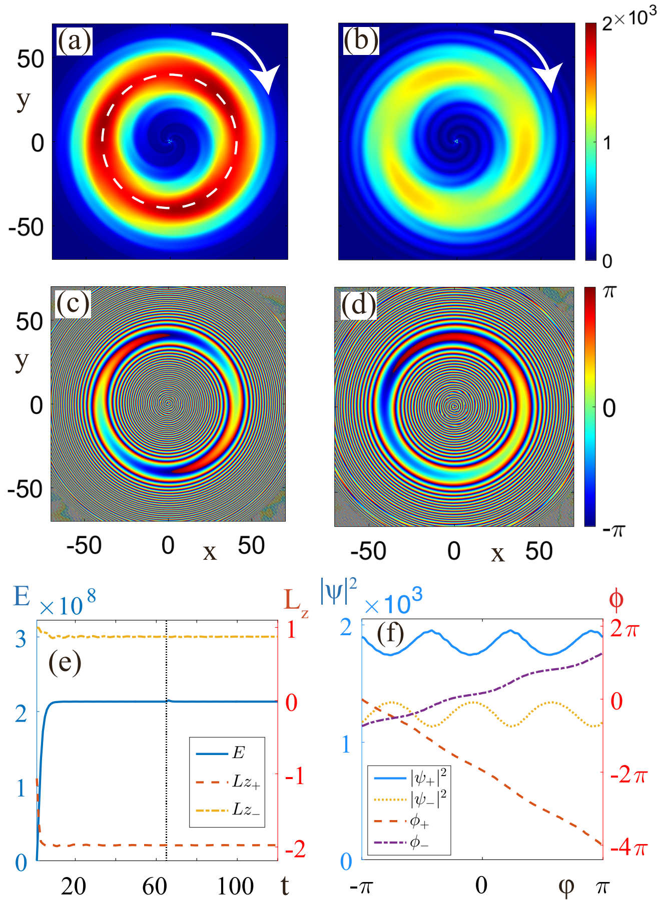

FIG. 2. Spatial distribution and time evolution of a soliton train state. (a) Density distribution for ψ_+. (b) Density distribution for ψ_-. White arrows indicate the rotation direction of the density dips. (c) Phase distribution for ψ_+. (d) Phase distribution for ψ_-. (e) Time evolution of the energy and normalized orbital angular momentum [6]. The vertical dotted line shows the perturbation added time. (f) Azimuthal distribution of density and phase along the dashed line in (a). The parameters are $\bar{P} = 25$, $P_L = 0.4$, $m_+ = -2$, $m_- = 1$, and $J = 0.17$.

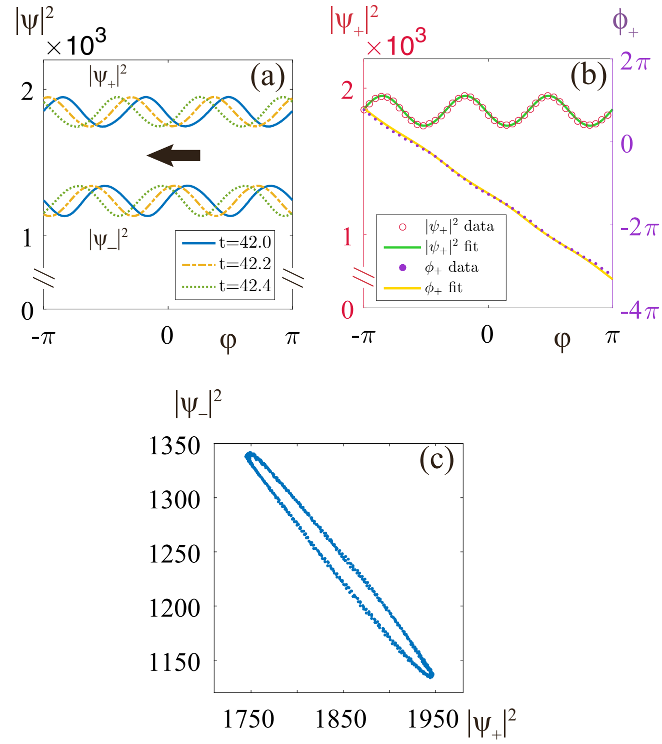

FIG. 3. (a) Azimuthal distribution of density for $\psi_\pm$ taken along the dashed ring in Fig. 2(a) at different times. (b) Fitted plots for the azimuthal density and phase distributions of ψ_+ at $t = 42.0$ (see the text). (c) Density dependence between two circularly polarized components at $t = 42.0$.

derived in [47,48],

$$|\psi_+(\varphi)|^2 \sim \mathrm{cn}^2(\tilde{\varphi},k), \quad \phi_+(\varphi) \sim \Pi(\xi,\tilde{\varphi},k), \tag{4}$$

where cn and Π are the Jacobi elliptic function and incomplete elliptic integral of the third kind, respectively, $\tilde{\varphi} = jK(k)(\varphi - \varphi_0)/\pi$ is the reduced azimuthal coordinate with j the number of density dips, φ_0 a constant phase shift, and $K(k)$ the complete elliptic integral of the first kind, where $k \in [0,1]$, and ξ are fitting parameters. In contrast to [48], instead of a linear dependence, the densities of the other component are related by the elliptic relation $[|\psi_+(\varphi)|^2]^2/a + [|\psi_-(\varphi)|^2]^2/b = 1$, where the numerical coefficients a and b define the axes of the ellipse (translated to the origin) shown in Fig. 3(c).

The phase winding number difference between two polarization components gives rise to circulating internal Josephson currents that form the Josephson vortex [17–19]. The expression of the internal Josephson current for polariton systems is given by [34]

$$I_J(\mathbf{r},t) = |\psi_+||\psi_-|\sin(\theta), \tag{5}$$

where θ is the relative phase defined in Eq. (3) and the positive value of I_J indicates particle flows from the $-$ component toward the $+$ component and vice versa. Figures 4(a) and 4(b) show the corresponding θ and I_J of the ST state in Fig. 2. Both of them are time dependent and rotating at the same speed as the cnodial wave. In contrast to the optical vortex azimuthon, the topological charge [52] of I_J has the same value as the number of the density dips in the azimuthal density distribution, specifically, 3 in our case. Here we emphasis that, unlike azimuthons supported purely by nonlinear interactions [36–38], the ST states we are considering are supported by the Josephson vortex given by the Josephson (linear) coupling.

The rotating Josephson vortex enables the realization of spin waves proposed recently in Ref. [25] for polariton systems. The spatial propagation of spin waves manifests itself in the linearly polarized basis [53]. As shown in Figs. 4(c) and 4(d), in the linearly polarized basis both H and V components of the ST state exhibit periodic density modulation with high contrast. The modulated densities, which rotate at the same speed as the density dips in Fig. 3(a), represent the optical ferris wheels [21] in cavity photoluminescence. They might be applicable in the design of a polariton spin switch [54] for ultrafast polaritonic devices.

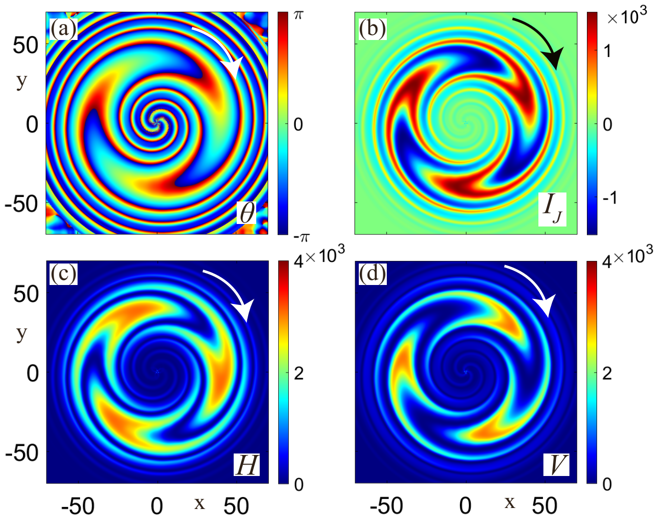

FIG. 4. Properties of the ST state shown in Fig. 2. Spatial distributions of (a) the relative phase θ and (b) the Josephson current I_J. Density distributions in the linearly polarized basis for (c) the horizontal H component and (d) the vertical V component. Arrows indicate rotation direction.

V. PATTERN FORMATION

It is well known that both self-interference effects and nonlinear instabilities in driven-dissipative systems can lead to the formation of stationary and fluctuating patterns [55,56]. In polariton systems, pattern formations have been observed in experiments, e.g., the sunflower state [57] and the self-ordered state [58]. Recently, it was proposed that modulational instability can result in the appearance of phase defects in polariton systems [59]. As it will be shown below, similarly, instabilities introduced by the Josephson vortex can lead to pattern formation in the density and phase for a polariton condensate.

With an increase of the linear coupling J, particle densities carried by the internal Josephson current become comparable to the azimuthal flow within each polarization component, so they can break the azimuthal flow by perturbations in the form of long thin stripes with sharp phase gradients. Figure 5 shows snapshots of nonstationary striped states. While both components keep their overall azimuthal flows, their density distributions are cut by density stripes that either originate from the center of the condensate (open stripe) or form a closed loop (closed stripe). Similar to the Faraday waves observed in atomic BEC systems [60–62], the stripes are oriented perpendicular across the condensate ring.

The locations of those density stripes are determined by that of the Josephson vortices, which is linked to the relative phase θ. Figures 5(d)–5(f) show the corresponding spatial distribution of $\theta(\mathbf{r})$. As we can see, the stripes are distributed randomly on top of a uniform phase background, which corresponds to a fixed relative phase θ_s, i.e., that of the SAB state. In the transverse direction of every stripe, the relative phase has a 2π phase change that consists of two π phase changes in both polarization components separately. Within a given polarization component, if its particle flow is represented as a path with directions, then when the path crosses the boundary of a stripe there will be a π phase change for the flow. Specifically, Fig. 6(a) shows a magnified plot for the relative phase in the area highlighted by a white box in Fig. 5 and a schematic plot of a path crossing the closed stripe. There are π phase changes with opposite sign for both components when the path passes the marked points A and B. The overall effect is that the path has zero phase gain after crossing the boundary of a closed stripe twice. Therefore, the phase winding number for each polarization component will not change by passing through a closed stripe. In contrast, open stripes that originate from the middle of the condensate toward the outside of the pumping region, as in Fig. 5(f), can change the phase winding number.

The Josephson vortex embodied in a stripe stems from differences in particle flows within two polarization components. Figure 6(c) shows a pseudo-three-dimensional plot for the Josephson current I_J corresponding to Fig. 6(a). The x-y plane represents the two-dimensional spatial distribution of I_J, where the darker and lighter colors indicate the positive and negative values of I_J, respectively. The $+$ component is placed above the plane, while the $-$ component is below the plane. The dark solid arrow (above the plane) indicates the particle flow in ψ_+ when passing through the boundary of the stripe (straight dashed line); the gray dashed arrow (below the plane) indicates the particle flow in ψ_- at the same position, where both components share approximately the same flow direction as indicated. The difference between the speed of two flows, which in turn leads to a 2π phase change in θ, results in the appearance of internal Josephson currents around the boundary of the stripe. Whereas particles tunnel from ψ_- to ψ_+ in the darker blue area (red arrow), the direction of the tunneling flow reverses in the lighter color area (green arrows), thus forming the Josephson vortex. Unlike the ST state and many superconducting systems where the Josephson vortex is given by tunneling between two counterpropagating flows [20], here it is given by tunneling between two copropagating flows. In addition, both its amplitude and position are time dependent. With the continuous change of the spatial distribution of particle flows in $\psi_\pm$, the position of the closed stripe will

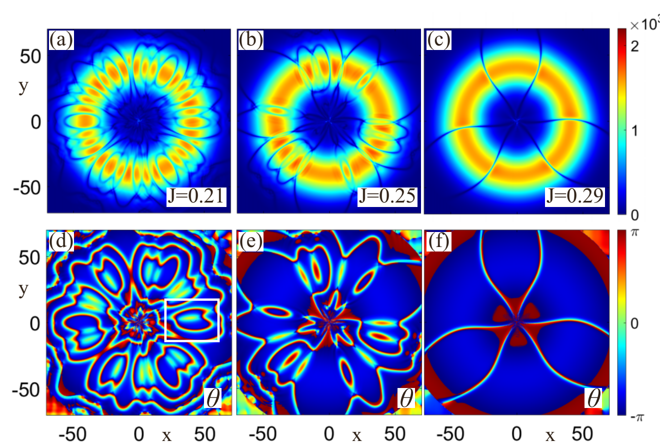

FIG. 5. (a)–(c) Density distribution of the less pumped component $|\psi_-|^2$ for different J. (d)–(f) Corresponding relative phase distribution. The white box indicates the magnification area shown in Fig. 6(a). The other parameters are the same as in Fig. 2.

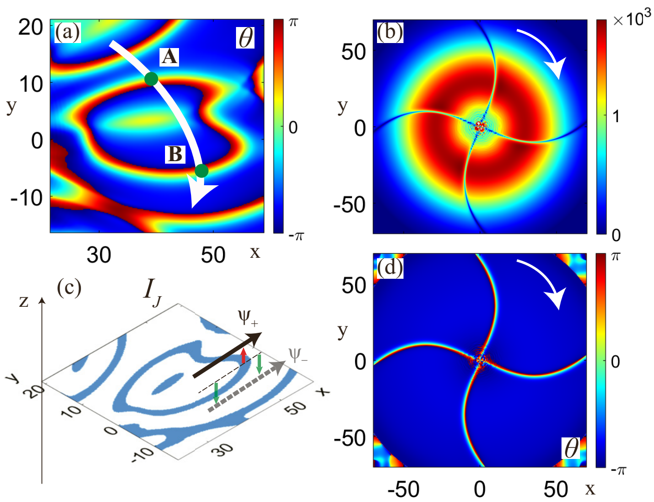

FIG. 6. (a) Magnified relative phase plot. The white arrow is a schematic illustration of a path having phase changes when crossing the boundary (green dots) of a closed stripe. (b) Density $|\psi_-|^2$ distribution of a steadily rotating striped state. (c) Schematic diagram showing the flow direction of the internal Josephson current (see the text). (d) Relative phase distribution of a steadily rotating striped state. White arrows in (b) and (d) indicate the rotation direction. The parameters are the same as in Fig. 2 except that $m_+ = -2$, $m_- = 2$, and $J = 0.26$.

change as a result. For the current case [Fig. 6(a)] the closed stripe will expand or merge with another closed stripe until it disappears.

Clearly, in this system the Josephson vortex has unconventional flow properties. However, we retain the terminology because of the same physical origin, i.e., circular exchange of the particle due to the linear coupling.

With a further increase of the linear coupling J, the effect of the SAB state is more obvious. As can be seen in Fig. 5, fewer density dips and relative phase stripes form with larger J and the phase becomes more uniform across the pumped area. In Fig. 5(e) the number of closed stripes reduces significantly, while keeping the number of open stripes the same (equal to the number of density dips in Fig. 2). This means that the overall phase winding number for each component can still be different from each other. In Fig. 5(f) no closed stripes exist and the number of open stripes is not equal to 3. In this case, both components share the same phase winding number and such a state is very close to the SAB state. The remaining open stripes are not static. They appear and collide with each other and disappear periodically.

A different set of parameters supports the existence of steady rotating stripes. Figures 6(b) and 6(d) show such an example. Four stripes rotated counterclockwise steadily, with the period at about $t = 96$ ps. Also, the arrangement for the 2π phase change direction in θ embodied in the stripes differs from that of Fig. 5(f), preventing them from merging. As the linear coupling J increases further, the condensate falls into the SAB state independently of the initial winding number in each component and the relative phase is fixed at θ_s everywhere.

A distinction should be made between defects in the relative phase of the striped states and the shock line defects in frozen states which are solutions of the complex Ginzburg-Landau equation [63,64]. The shock line defects are caused by the phase difference between two nearby vortices [63,64], which are basically single-component phenomena for an open-dissipative system. In fact, shock lines and frozen states have been observed numerically for a single-component polariton condensate under a homogeneous incoherent pump in [59]. In addition, it has been observed in experiment that a spiraling state called the sunflower state [57] exists under a Gaussian-shape incoherent pump, which might correspond to the frozen states after spiraling waves are established [59]. In contrast, the striped states considered here are intrinsically two-component phenomena that highly depend on the strength of the linear coupling J (see Fig. 5).

Note that Eq. (1) only considers the same-spin condensate-reservoir interaction [9,50]. If the cross-spin condensate-reservoir interaction were included, assuming that it has the same strength as the same-spin one, the interaction would change the parameter regimes of vortex states, azimuthons, and patterned states.

The competition between the nonlinear interaction and the linear coupling is ubiquitous in many multicomponent nonlinear systems. Thus, the pattern formation leading to striped states could be applicable to other dissipative nonlinear systems such as atomic BECs and nonlinear optics.

VI. SPONTANEOUS VORTEX GENERATION

In the two preceding sections, the orbital angular momentum (OAM) of each component was imprinted by an external coherent LG pulse in the initial stage of the condensate evolution towards a steady state. While ensuring the controlled generation of angular momentum, this coherent imprinting is not essential for obtaining nonzero OAM for a polariton condensate. In fact, each component can acquire angular momentum independently starting from white noise in the process of mode selection governed by the specific spatial configuration of the incoherent pump [65]. In this section we will show the process of ST state generation from white noise. In addition, the final state will exhibit an asymmetric density distribution due to the random capture of the initially formed vortices.

We start by discussing generally the condensate growing process that applies to a wide range of pumping configurations. This process, which is governed by the model equations (1), is essentially a single-component phenomenon and can be illustrated by the example of a polariton condensate supported by a fully circularly polarized pump ($P_L = 0$). In this case the pumped polarization component $\psi = \psi_+$ dominates the whole dynamical process. Before the pump reaches the threshold power, the particle density $|\psi|^2$ is zero or takes a negligibly small value. When the pumping threshold power is reached, the $|\psi|^2 = 0$ state is no longer dynamically stable and the condensate density will grow exponentially [66,67]. If we assume that the correlation length of ψ extends to the whole pumped region, then ψ will grow like $\psi \sim |\psi_0| e^{i\phi_0} e^{i\omega_1 t} e^{\omega_2 t}$, where ϕ_0 is the initial phase and $\omega_{1,2}$ are the real and imaginary parts of the eigenfrequency of the unstable mode, respectively [6]. This is a typical homogeneous growth scenario where the whole condensate shares the same growth rate (given by

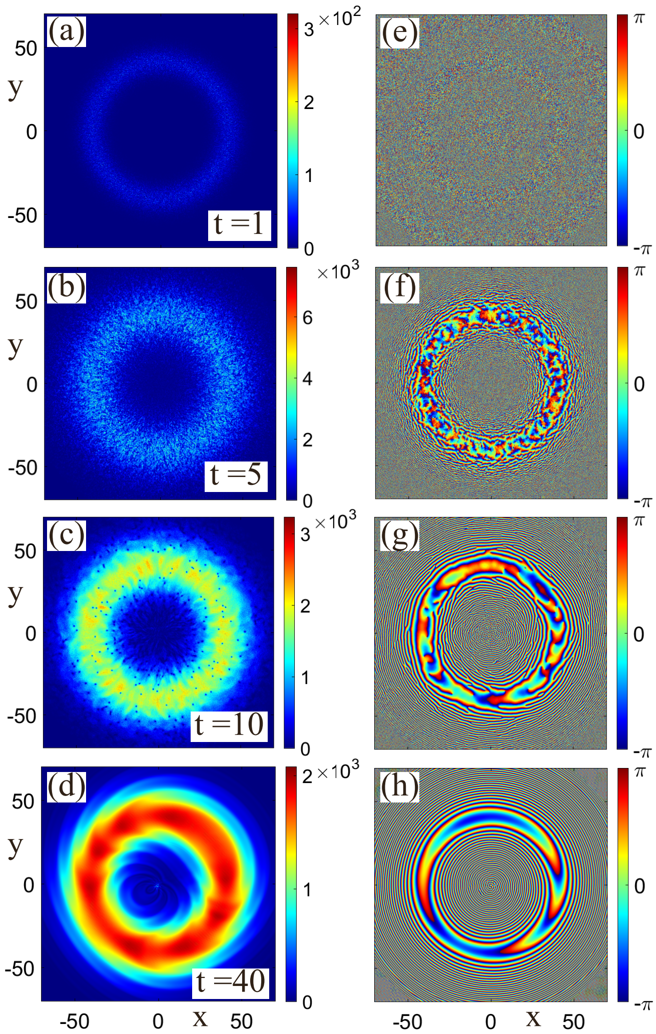

FIG. 7. Inhomogeneous growth of the condensate and spontaneous formation of a vortex state. (a)–(d) Density distribution of $|\psi_+|^2$. (e)–(h) Phase distribution ϕ_+ for the corresponding time.

ω_2) and the final state would inherit the angular momentum completely from ϕ_0 (under a radially symmetric pump). If ϕ_0 has no OAM, then there is none in the final state.

When noise is present in the initial state or in the driven-dissipative GP equation, the condensate will experience inhomogeneous growth and vortices will appear. A practical white noise can be generated independently at each point from a random variable $Y = n_s X$, where the random variable $X \sim N(0,1)$ follows the standard normal distribution [68] and n_s represents the noise strength. Depending on the noise strength, the noise in the phase of the condensate will reduce the correlation length of the condensate and when n_s reaches a critical value, the correlation length becomes zero and thus the growth rate of the condensate will differ from point to point. Localized defects such as vortices can form during this process.

With the continuous growth of the condensate, those initial vortices will be captured or repelled by the condensate depending on the specific pumping configuration. Figure 7 shows snapshots of the inhomogeneous growth of the condensate and the spontaneous formation of vortices. The condensate is seeded by a sufficiently strong white noise. As we can see from Figs. 7(a)–7(c), vortices grow locally and are randomly captured within the pumped ring. Vortices with opposite charges annihilate and if they do not cancel out completely, the remaining charge will be inherited by the bulk condensate as in Fig. 7(d). Note that in Fig. 7 the linear Josephson coupling J is set to support a ST state. The spontaneous formation of vorticity for each component can be regarded as independent from each other for the current pumping configuration. The resulting state is an imperfect azimuthon vortex state. The same process also applies to spontaneous formation of homogeneous vortex states and striped states.

VII. CONCLUSION

In conclusion, by using a dynamical mean-field model to describe a two-component exciton-polariton condensate formed in the incoherent spin-polarized pumping regime, we have demonstrated the existence and dynamical stability of vortex azimuthons and spin patterns in an annular trapping geometry imposed by the pumping geometry. We have investigated the intrinsic connection between these nontrivial spin structures and internal Josephson currents supported by a linear polarization splitting. In experiments, the polarization splitting can be controlled by different methods, e.g., by applying stress [69], electric fields [70], or magnetic fields [71]. It has been reported that the polarization splitting can reach 0.2 meV [73]; when normalized by $E_u = 0.66$ meV, it corresponds to $J = 0.3$, high enough to support azimuthons (cf. $J = 0.17$ in Fig. 2). Therefore, it is feasible to observe azimuthons with the existing experimental techniques. With a given value of polarization splitting, one can tune other parameters, e.g., the polarization bias of the incoherent pump, to probe different regimes. Our results are generally applicable to other open-dissipative systems in the context of atomic BECs and nonlinear optics.

ACKNOWLEDGMENTS

This work was supported by the Australian Research Council and the China Scholarship Council. The author thanks Michael Fraser, Alexey Yulin, and Elena A. Ostrovskaya for useful discussions and in-depth comments.

[1] I. Carusotto and C. Ciuti, Rev. Mod. Phys. **85**, 299 (2013).
[2] C. Schneider, K. Winkler, M. D. Fraser, M. Kamp, Y. Yamamoto, E. A. Ostrovskaya, and S. Hoefling, arXiv:1510.07540.
[3] T. Byrnes, N. Y. Kim, and Y. Yamamoto, Nat. Phys. **10**, 803 (2014).
[4] F. Manni, K. G. Lagoudakis, T. C. H. Liew, R. André, and B. Deveaud-Plédran, Phys. Rev. Lett. **107**, 106401 (2011).
[5] A. Dreismann, P. Cristofolini, R. Balili, G. Christmann, F. Pinsker, N. G. Berloff, Z. Hatzopoulos, P. G. Savvidis, and J. J. Baumberg, Proc. Natl. Acad. Sci. USA **111**, 8770 (2014).

[6] G. Li, M. D. Fraser, A. Yakimenko, and E. A. Ostrovskaya, Phys. Rev. B **91**, 184518 (2015).
[7] G. Liu, D. W. Snoke, A. Daley, L. N. Pfeiffer, and K. West, Proc. Natl. Acad. Sci. USA **112**, 2676 (2015).
[8] K. G. Lagoudakis, T. Ostatnický, A. V. Kavokin, Y. G. Rubo, R. André, and B. Deveaud-Plédran, Science **326**, 974 (2009).
[9] E. Kammann, T. C. H. Liew, H. Ohadi, P. Cilibrizzi, P. Tsotsis, Z. Hatzopoulos, P. G. Savvidis, A. V. Kavokin, and P. G. Lagoudakis, Phys. Rev. Lett. **109**, 036404 (2012).
[10] R. Hivet, H. Flayac, D. D. Solnyshkov, D. Tanese, T. Boulier, D. Andreoli, E. Giacobino, J. Bloch, A. Bramati, G. Malpuech, and A. Amo, Nat. Phys. **8**, 724 (2012).
[11] F. Manni, Y. Léger, Y. G. Rubo, R. André, and B. Deveaud, Nat. Commun. **4**, 2590 (2013).
[12] P. Cilibrizzi, H. Sigurdsson, T. C. H. Liew, H. Ohadi, S. Wilkinson, A. Askitopoulos, I. A. Shelykh, and P. G. Lagoudakis, Phys. Rev. B **92**, 155308 (2015).
[13] I. A. Shelykh, A. V. Kavokin, and G. Malpuech, Phys. Status Solidi B **242**, 2271 (2005).
[14] A. Kavokin, G. Malpuech, and M. Glazov, Phys. Rev. Lett. **95**, 136601 (2005).
[15] M. O. Borgh, J. Keeling, and N. G. Berloff, Phys. Rev. B **81**, 235302 (2010).
[16] G. Li, T. C. H. Liew, O. A. Egorov, and E. A. Ostrovskaya, Phys. Rev. B **92**, 064304 (2015).
[17] V. M. Kaurov and A. B. Kuklov, Phys. Rev. A **71**, 011601(R) (2005).
[18] S.-W. Su, S.-C. Gou, A. Bradley, O. Fialko, and J. Brand, Phys. Rev. Lett. **110**, 215302 (2013).
[19] S.-W. Su, S.-C. Gou, I.-K. Liu, A. S. Bradley, O. Fialko, and J. Brand, Phys. Rev. A **91**, 023631 (2015).
[20] D. Roditchev, C. Brun, L. Serrier-Garcia, J. C. Cuevas, V. H. L. Bessa, M. V. Milošević, F. Debontridder, V. Stolyarov, and T. Cren, Nat. Phys. **11**, 332 (2015).
[21] S. Franke-Arnold, J. Leach, M. J. Padgett, V. E. Lem-bessis, D. Ellinas, A. J. Wright, J. M. Girkin, P. Öhberg, and A. S. Arnold, Opt. Express **15**, 8619 (2007).
[22] K. Rayanov, B. L. Altshuler, Y. G. Rubo, and S. Flach, Phys. Rev. Lett. **114**, 193901 (2015).
[23] M. Wouters and I. Carusotto, Phys. Rev. Lett. **99**, 140402 (2007).
[24] M. Vladimirova, S. Cronenberger, D. Scalbert, K. V. Kavokin, A. Miard, A. Lemaître, J. Bloch, D. Solnyshkov, G. Malpuech, and A. V. Kavokin, Phys. Rev. B **82**, 075301 (2010).
[25] M. M. Glazov and A. V. Kavokin, Phys. Rev. B **91**, 161307(R) (2015).
[26] H. Ohadi, A. Dreismann, Y. G. Rubo, F. Pinsker, Y. del Valle-Inclan Redondo, S. I. Tsintzos, Z. Hatzopoulos, P. G. Savvidis, and J. J. Baumberg, Phys. Rev. X **5**, 031002 (2015).
[27] In the numerical calculations, the following values of parameters are chosen as experimentally accessible [72]: $m_{LP} = 10^{-4} m_e$ (where m_e is the free electron mass), $u_a = 6 \times 10^{-3}$ meV μm^2, $u_b = -0.1 u_a$, $g_R = 2u_a$, $\gamma_c = 0.33$ ps^{-1}, $\gamma_R = 1.5\gamma_c$, $R = 0.01$ μm^2 ps^{-1}, and $J \approx 0.01 \sim 0.5$ meV [73]. So the dimensionless quantities are $u_a = 7.7 \times 10^{-3}$, $u_b = -7.7 \times 10^{-4}$, $g_R = 1.5 \times 10^{-2}$, $\gamma_R = 1.5$, $R = 8.4 \times 10^{-3}$, and $J \approx$ 0.01–0.5. This choice of parameters corresponds to an assumption of a very short lifetime of reservoir excitons, however the results do not depend on the particular value of γ_R.
[28] W. Bao and Y. Cai, Kinet. Relat. Mod. **6**, 1 (2013).
[29] J. Javanainen and J. Ruostekoski, J. Phys. A **39**, L179 (2006).
[30] Y. G. Rubo, Phys. Rev. Lett. **99**, 106401 (2007).
[31] M. Toledo-Solano, M. E. Mora-Ramos, A. Figueroa, and Y. G. Rubo, Phys. Rev. B **89**, 035308 (2014).
[32] F. Manni, K. G. Lagoudakis, T. C. H. Liew, R. André, V. Savona, and B. Deveaud, Nat. Commun. **3**, 1309 (2012).
[33] H. Terças, H. Flayac, D. D. Solnyshkov, and G. Malpuech, Phys. Rev. Lett. **112**, 066402 (2014).
[34] M. Wouters, Phys. Rev. B **77**, 121302(R) (2008).
[35] D. Sanvitto, F. M. Marchetti, M. H. Szymańska, G. Tosi, M. Baudisch, F. P. Laussy, D. N. Krizhanovskii, M. S. Skolnick, L. Marrucci, A. Lemaître, J. Bloch, C. Tejedor, and L. Viña, Nat. Phys. **6**, 527 (2010).
[36] A. S. Desyatnikov, A. A. Sukhorukov, and Y. S. Kivshar, Phys. Rev. Lett. **95**, 203904 (2005).
[37] S. Lopez-Aguayo, A. S. Desyatnikov, and Y. S. Kivshar, Opt. Express **14**, 7903 (2006).
[38] V. M. Lashkin, E. A. Ostrovskaya, A. S. Desyatnikov, and Y. S. Kivshar, Phys. Rev. A **80**, 013615 (2009).
[39] A. Minovich, D. N. Neshev, A. S. Desyatnikov, W. Krolikowski, and Y. S. Kivshar, Opt. Express **17**, 23610 (2009).
[40] Y. V. Izdebskaya, A. S. Desyatnikov, G. Assanto, and Y. S. Kivshar, Opt. Express **19**, 21457 (2011).
[41] V. E. Lobanov, Y. V. Kartashov, V. A. Vysloukh, and L. Torner, Opt. Lett. **36**, 85 (2011).
[42] O. V. Borovkova, V. E. Lobanov, Y. V. Kartashov, and L. Torner, Opt. Lett. **36**, 1936 (2011).
[43] O. V. Borovkova, V. E. Lobanov, Y. V. Kartashov, and L. Torner, Phys. Rev. A **85**, 023814 (2012).
[44] E. A. Ostrovskaya, J. Abdullaev, A. S. Desyatnikov, M. D. Fraser, and Y. S. Kivshar, Phys. Rev. A **86**, 013636 (2012).
[45] L. D. Carr, C. W. Clark, and W. P. Reinhardt, Phys. Rev. A **62**, 063610 (2000).
[46] L. D. Carr, C. W. Clark, and W. P. Reinhardt, Phys. Rev. A **62**, 063611 (2000).
[47] R. Kanamoto, L. D. Carr, and M. Ueda, Phys. Rev. A **79**, 063616 (2009).
[48] J. Smyrnakis, M. Magiropoulos, G. M. Kavoulakis, and A. D. Jackson, Phys. Rev. A **87**, 013603 (2013).
[49] A. M. Kamchatnov, Y. V. Kartashov, P.-É. Larré, and N. Pavloff, Phys. Rev. A **89**, 033618 (2014).
[50] F. Pinsker and H. Flayac, Phys. Rev. Lett. **112**, 140405 (2014).
[51] R. Atre, P. K. Panigrahi, and G. S. Agarwal, Phys. Rev. E **73**, 056611 (2006).
[52] D. J. Thouless, *Topological Quantum Numbers in Nonrelativistic Physics* (World Scientific, Singapore, 1998).
[53] M. Ö. Oktel and L. S. Levitov, Phys. Rev. Lett. **88**, 230403 (2002).
[54] A. Amo, T. C. H. Liew, C. Adrados, R. Houdré, E. Giacobino, A. V. Kavokin, and A. Bramati, Nat. Photon. **4**, 361 (2010).
[55] M. C. Cross and P. C. Hohenberg, Rev. Mod. Phys. **65**, 851 (1993).
[56] K. Staliunas and V. J. Sánchez-Morcillo, *Transverse Patterns in Nonlinear Optical Resonators* (Springer, Berlin, 2003).
[57] G. Christmann, G. Tosi, N. G. Berloff, P. Tsotsis, P. S. Eldridge, Z. Hatzopoulos, P. G. Savvidis, and J. J. Baumberg, Phys. Rev. B **85**, 235303 (2012).
[58] F. Manni, T. C. H. Liew, K. G. Lagoudakis, C. Ouellet-Plamondon, R. André, V. Savona, and B. Deveaud, Phys. Rev. B **88**, 201303(R) (2013).

[59] T. C. H. Liew, O. A. Egorov, M. Matuszewski, O. Kyriienko, X. Ma, and E. A. Ostrovskaya, Phys. Rev. B **91**, 085413 (2015).
[60] P. Engels, C. Atherton, and M. A. Hoefer, Phys. Rev. Lett. **98**, 095301 (2007).
[61] A. Balaž and A. I. Nicolin, Phys. Rev. A **85**, 023613 (2012).
[62] A. Balaž, R. Paun, A. I. Nicolin, S. Balasubramanian, and R. Ramaswamy, Phys. Rev. A **89**, 023609 (2014).
[63] I. S. Aranson and L. Kramer, Rev. Mod. Phys. **74**, 99 (2002).
[64] C. Brito, I. S. Aranson, and H. Chaté, Phys. Rev. Lett. **90**, 068301 (2003).
[65] A. Yulin, A. S. Desyatnikov, and E. A. Ostrovskaya (unpublished).
[66] U. C. Täuber and S. Diehl, Phys. Rev. X **4**, 021010 (2014).
[67] M. Matuszewski and E. Witkowska, Phys. Rev. B **89**, 155318 (2014).
[68] A. Papoulis, *Probability, Random Variables and Stochastic Processes*, 3rd ed. (McGraw-Hill, New York, 1991).
[69] R. B. Balili, D. W. Snoke, L. Pfeiffer, and K. West, Appl. Phys. Lett. **88**, 031110 (2006).
[70] G. Malpuech, M. M. Glazov, I. A. Shelykh, P. Bigenwald, and K. V. Kavokin, Appl. Phys. Lett. **88**, 111118 (2006).
[71] A. V. Kavokin, M. Vladimirova, B. Jouault, T. C. H. Liew, J. R. Leonard, and L. V. Butov, Phys. Rev. B **88**, 195309 (2013).
[72] G. Roumpos, M. D. Fraser, A. Löffler, S. Höfling, A. Forchel, and Y. Yamamoto, Nat. Phys. **7**, 129 (2011).
[73] Ł. Kłopotowski, M. D. Martín, A. Amo, L. Viña, I. A. Shelykh, M. M. Glazov, G. Malpuech, A. V. Kavokin, and R. André, Solid State Commun. **139**, 511 (2006).